Supporting Information

Th@D_{5h}(6)-C$_{80}$: highly symmetric fullerene cage stabilized by a single metal ion

Yingjing Yan,[a†] Roser Morales-Martínez,[c†] Jiaxin Zhuang, [a†] Yang-Rong Yao,[b] Xiaomeng Li,[a] Josep M. Poblet,[c] Antonio Rodríguez-Fortea,[c]* and Ning Chen[a]*

[a] College of Chemistry, Chemical Engineering and Materials Science, and State Key Laboratory of Radiation Medicine and Protection, Soochow University, Suzhou, Jiangsu 215123, P.R. China.
[b] Department of Chemistry, The University of Texas at El Paso, 500 W University Avenue, El Paso, Texas 79968, United States
[c] Departament de Química Física i Inorgànica, Universitat Rovira i Virgili, Marcel·lí Domingo 1, 43007 Tarragona, Spain
Email: *chenning@suda.edu.cn*; antonio.rodriguezf@urv.cat

†These authors contribute equally to this work.

Table of Contents

■ **Experimental Details**

Experimental Details

Synthesis and isolation of Th@C$_{80}$. The carbon soot containing thorium EMFs was synthesized by the direct-current arc discharge method. The graphite rods, packed with ThO$_2$ powders and graphite powders (1:24 molar ratio), were vaporized in the arcing chamber under a 200 Torr He atmosphere. The resulting soot was refluxed in CS$_2$ under an argon atmosphere for 12 h. The separation and purification of Th@C$_{80}$ were achieved by multi-stage HPLC procedures. Multiple HPLC columns, including Buckyprep-M column (25 × 250 mm, Cosmosil, Nacalai Tesque Inc.), Buckprep-D column (10 × 250 mm, Cosmosil, Nacalai Tesque, Japan), and Buckprep column (10 × 250 mm, Cosmosil, Nacalai Tesque, Japan), were utilized in the procedures.

Spectroscopic and Electrochemical Studies. The positive-ion mode matrix-assisted laser desorption ionization time-of-flight (MALDI-TOF) (Bruker, Germany) was employed for the mass characterization. The UV-vis-NIR spectrum of the purified Th@C$_{80}$ was measured in CS$_2$ solution with a Cary 5000 UV-vis-NIR spectrophotometer (Agilent, USA). The Raman spectrum was obtained using a Horiba Lab RAM HR Evolution Raman spectrometer using a laser at 785 nm. Cyclic voltammetry (CV) results were obtained in *o*-dichlorobenzene using a CHI-660E instrument. A conventional three-electrode cell consisting of a platinum counter-electrode, a glassy carbon working electrode, and a silver reference electrode was used for the measurements. (*n*-Bu)$_4$NPF$_6$ (0.05 M) was used as supporting electrolyte. The CV were measured at the scan rate of 100 mV/s.

X-ray Crystallographic Study. The black block crystal of Th@C$_{80}$ was obtained by slow diffusion of the CS$_2$ solution of the corresponding metallofullerene compounds into the benzene solution of [Ni^{II}(OEP)]. Single-crystal X-ray data of Th@D_{5h}(6)-C$_{80}$ was collected at 113 K on a diffractometer (Bruker D8 Venture) equipped with a CCD collector. The multi-scan method was used for absorption correction. The structure was solved using direct methods[1] and refined on F^2 using full-matrix least-squares using the SHELXL2014[2] crystallographic software packages. Hydrogen atoms were inserted at calculated positions and constrained with isotropic thermal parameters.

Crystal data for Th@D_{5h}(6)-C$_{80}$·[Ni^{II}(OEP)]·1.5(C$_6$H$_6$) ·CS$_2$: M_r = 1977.59, 0.12 mm × 0.1 mm × 0.08 mm, monoclinic, $P2_1/c$ (No. 14), a = 17.5890(10) Å, b = 17.0252(10) Å, c = 26.7962(14) Å, α = 90°, β = 106.593(2)°, γ = 90°, V = 7690.1(7) Å^3, Z = 4, ρ_{calcd} = 1.708 g cm^{-3}, μ(CuKα) = 7.529 mm^{-1}, ϑ = 3.69-68.22, T = 113(2) K, R_1 = 0.0901, wR_2 = 0.2299 for all data; R_1 = 0.0874, wR_2 = 0.2275 for 13166 reflections (I > 2.0σ(I)) with 2017 parameters. Goodness-of-fit indicator 1.030. Maximum residual electron density 2.848 e Å^{-3}. The crystallographic data for this structure have been deposited at the Cambridge Crystallographic Data Centre (CCDC) with the deposition number 2048360.

High-performance liquid chromatography separation process of Th@D_{5h}(6)-C$_{80}$.

The first stage was performed on a Buckyprep-M column (25 mm × 250 mm, Cosmosil Nacalai Tesque) with toluene as mobile phase. After that, as shown in Fig. S1, fraction from 51 to 54.5 min (marked in blue) was re-injected into a Buckyprep-D column (10 mm × 250 mm, Cosmosil Nacalai Tesque) for the second stage separation using toluene as the eluent. Then, the fraction marked in light blue was collected. After concentrating, the third stage of separation was conducted on a Buckyprep column (10 mm × 250 mm, Cosmosil Nacalai Tesque) using toluene as the eluent, fraction on 80-87 min which containing of Th@C$_{80}$ was collected. The final stage was performed on a Buckyprep-D column (10 mm × 250 mm, Cosmosil Nacalai Tesque) and pure Th@C$_{80}$ marked in purple was finally obtained, along with the MALDI-TOF mass spectrometry in a positively charged mode (Fig. 1).
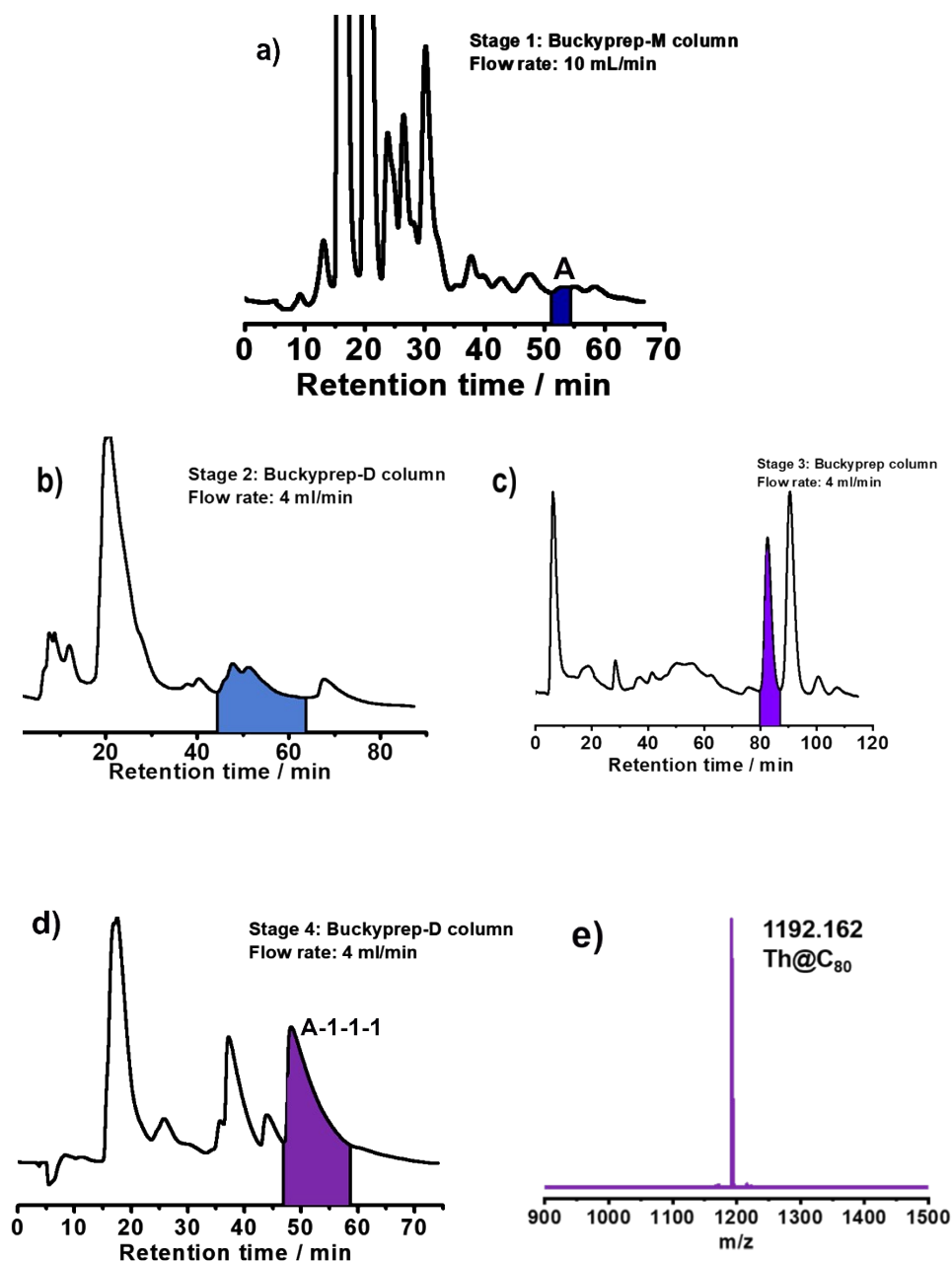
Fig. S1 HPLC profiles showing the separation procedures of Th@D_{5h}(6)-C$_{80}$. (a) The first stage HPLC chromatogram of extract on a Buckyprep-M column (Φ = 25 mm × 250 mm), (b) The second stage HPLC chromatogram of fraction A on a Buckyprep-D column (Φ = 10 mm × 250 mm), (c) The third stage HPLC chromatogram of fraction A-1 on a Buckyprep column (Φ = 10 mm × 250 mm), (d) The forth stage HPLC chromatogram of fraction A-1-1 on a Buckyprep-D column (Φ = 10 mm × 250 mm), The HPLC conditions were: eluent = toluene; detecting wavelength = 310 nm. (e) The single peak of Th@C$_{80}$, m/z at 1192.162 on positive-ion-mode matrix-assisted laser desorption-ionization time-of-flight mass spectrometry (MALDI-TOF MS).

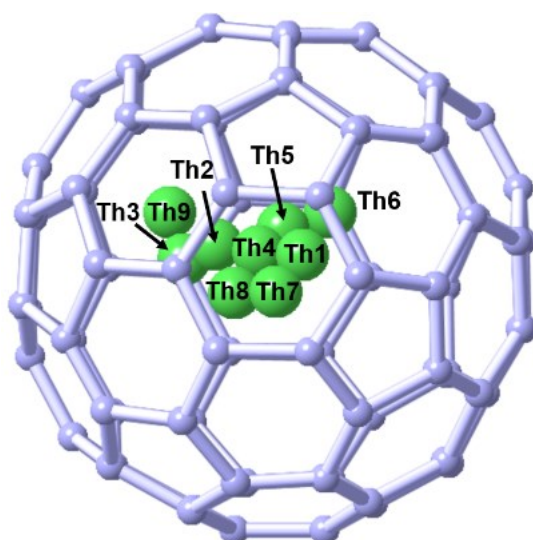**Fig. S2** Ball and stick representation of disordered Th sites in Th@D_{5h}(6)-C$_{80}$. For clarity, only the major cage orientations is shown.

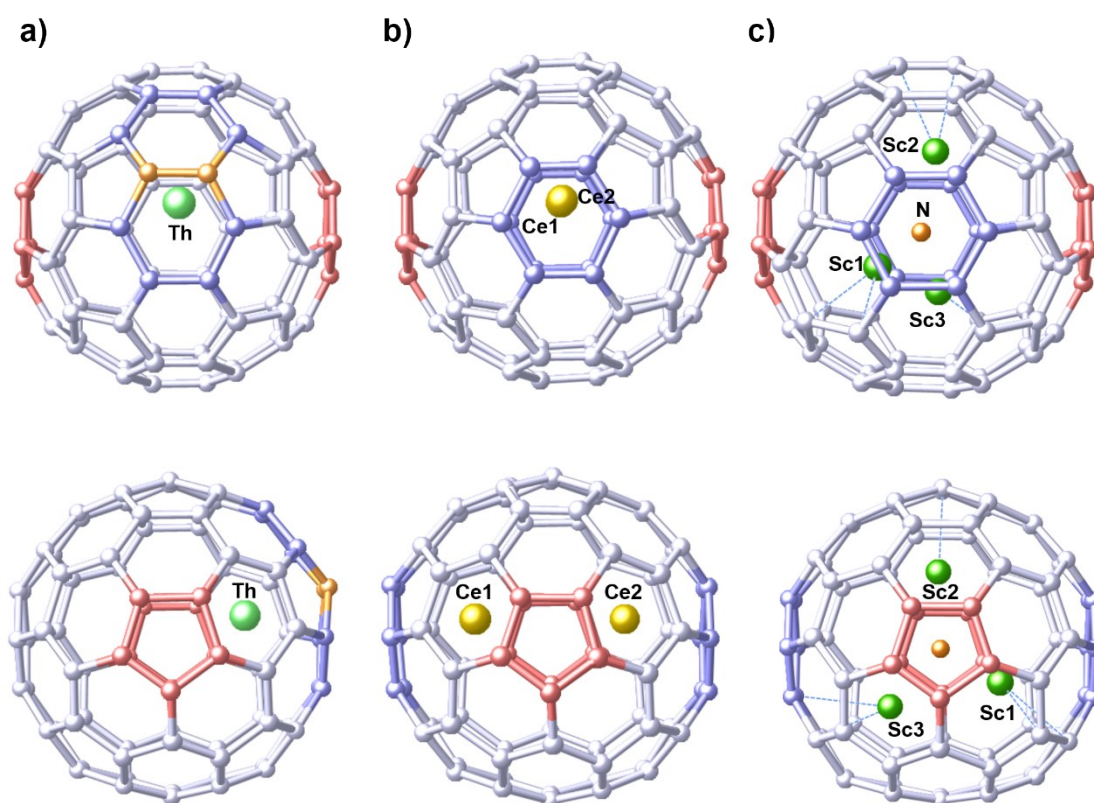**Fig. S3** Molecular structure of (a) Th@D_{5h}(6)-C$_{80}$, (b) Ce$_2$@D_{5h}(6)-C$_{80}$,[3] (c) Sc$_3$N@D_{5h}(6)-C$_{80}$.[4] The 5-fold axis of D_{5h}(6)-C$_{80}$ is aligned horizonally (top) and vertically (down) to the plane, respectively.

Table S1. Occupancies of disordered thorium sites in Th@D_{5h}(6)-C$_{80}$.

Labelling	Th1	Th2	Th3	Th4	Th5
Occupancy	0.421(5)	0.196(3)	0.125(3)	0.111(3)	0.068(4)
Labelling	**Th6**	**Th7**	**Th8**	**Th9**	
Occupancy	0.0237(8)	0.0191(13)	0.0198(10)	0.0170(7)	

Table S2. Closest Th-C contacts in Th-based mono-EMFs.

Compound	Th-C distance / Å	major Th site position	Ref
Th@D_{5h}(6)-C$_{80}$	2.326/2.327	under the [6, 6] bond of a corannulene ring	this work
Th@C_{3v}(8)-C$_{82}$	2.340(14)-2.494(10)	under the intersection of three hexagons	5
Th@C_1(28324)-C$_{80}$	2.366-2.544	close to the edge of the fused pentagon pair	6
Th@C_1(11)-C$_{86}$	2.326-2.457	under a sumanene-type hexagon	7
Th@T_d(19151)-C$_{76}$	2.390(13)-2.466(13)	under a sumanene-type hexagon	8

Table S3. Redox potentials (V vs. Fc/Fc$^+$) and electrochemical band gaps of Th@D_{5h}(6)-C$_{80}$ and the selected reference EMFs.

Compounds	E$^{2+/+}$	E$^{+/0}$	E$^{0/-}$	E$^{-/2-}$	E$^{2-/3-}$	E$_{gap,ec}$(V)	Ref
Th@D_{5h}(6)-C$_{80}$	0.92[b]	0.26[a]	-0.63[a]	-0.95[a]	-1.86[a]	0.89	this work
Th@C_1(28324)-C$_{80}$		0.24[a]	-1.22[b]	-1.50[a]	-2.05[a]	1.46	6
Th@T_d(19151)-C$_{76}$	0.75[b]	0.03[a]	-1.04[a]	-1.41[a]	-1.78[a]	1.07	8
Th@C_{3v}(8)-C$_{82}$		0.46[a]	-1.05[b]	-1.54[b]	-1.69[b]	1.51	5
Th@C_1(11)-C$_{86}$		0.21[a]	-1.17[a]	-1.51[a]	-1.85[a]	1.38	7
Ce$_2$@D_{5h}(6)-C$_{80}$	0.66[a]	0.20[a]	-0.40[a]	-1.76[a]	-2.16[a]	0.60	3
Lu$_3$N@D_{5h}(6)-C$_{80}$	0.64[a]	0.31[a]	-1.47[a]	-1.95[b]		1.78	9

[a] Half-wave potential (reversible redox process). [b] Peak potential (irreversible redox process).

Computational Details

All the calculations were carried out using density functional theory (DFT) with the ADF 2017 package.[10] The PBE0 functional [11, 12] and Slater triple-zeta polarization basis sets (PBE0-DG3/TZP) were used, including Grimme dispersion corrections.[13] Frozen cores consisting of the 1s shell for C and the 1s to 5d shells for Th were described by means of single Slater functions. Scalar relativistic corrections were included by means of the ZORA formalism. Frequency calculations and Raman spectrum were obtained using PBE functional and TZP basis set.[14] Oxidation and reduction potentials were computed using a standard methodology for endohedral metallofullerenes (BP86/TZP).[4] Different positions of the Th atom inside the $D_{5h}(6)$-C_{80} cage were considered and optimized at first PBE/TZP level and then at PBE0/TZP level (see Table S4).

Table S4. Relative energies (kcal mol^{-1}) at PBE0 and PBE levels for different positions of Th atom inside $D_{5h}(6)$-C_{80} cage.^{a}

Position	PBE	PBE0	Initial position	Final position
1	0.0	0.0	[6, 6] bond in a pyracylene motif	[6, 6] bond in a pyracylene motif
2	12.6	13.8	Intersection of three hexagons	Center of a hexagon in an s-indacene motif
3	15.8	16.4	[6, 6] bond between a 665 and a 666 C atoms	Center of a hexagon in an s-indacene motif
4	0.0	0.0	Center of a hexagon in a pyracylene motif	[6, 6] bond in a pyracylene motif

Due to the high symmetry of the $D_{5h}(6)$-C_{80} cage there are several equivalent Th positions inside the cage. Besides the position obtained from the X-ray structure (position 1), we have initially located the Th atom at the intersection of three hexagons (triple hexagon junction or THJ, position 2), under a [6,6] bond between a corannulene (665) and a pyrene (666) C atom (position 3) and in the center of a hexagon in a pyracylene motif (position 4). Once the geometry was optimized, the Th atom in position 2 moved to near the center of a hexagon in an s-indacene motif, at higher energy compared to the location under the [6, 6] bond in a pyracylene motif. Th atom in position 3 also moved to near the center of a hexagon in an s-indacene motif. Th atom in position 4 moved under the [6, 6] bond in a pyracylene motif, the position observed in the X-ray structure.
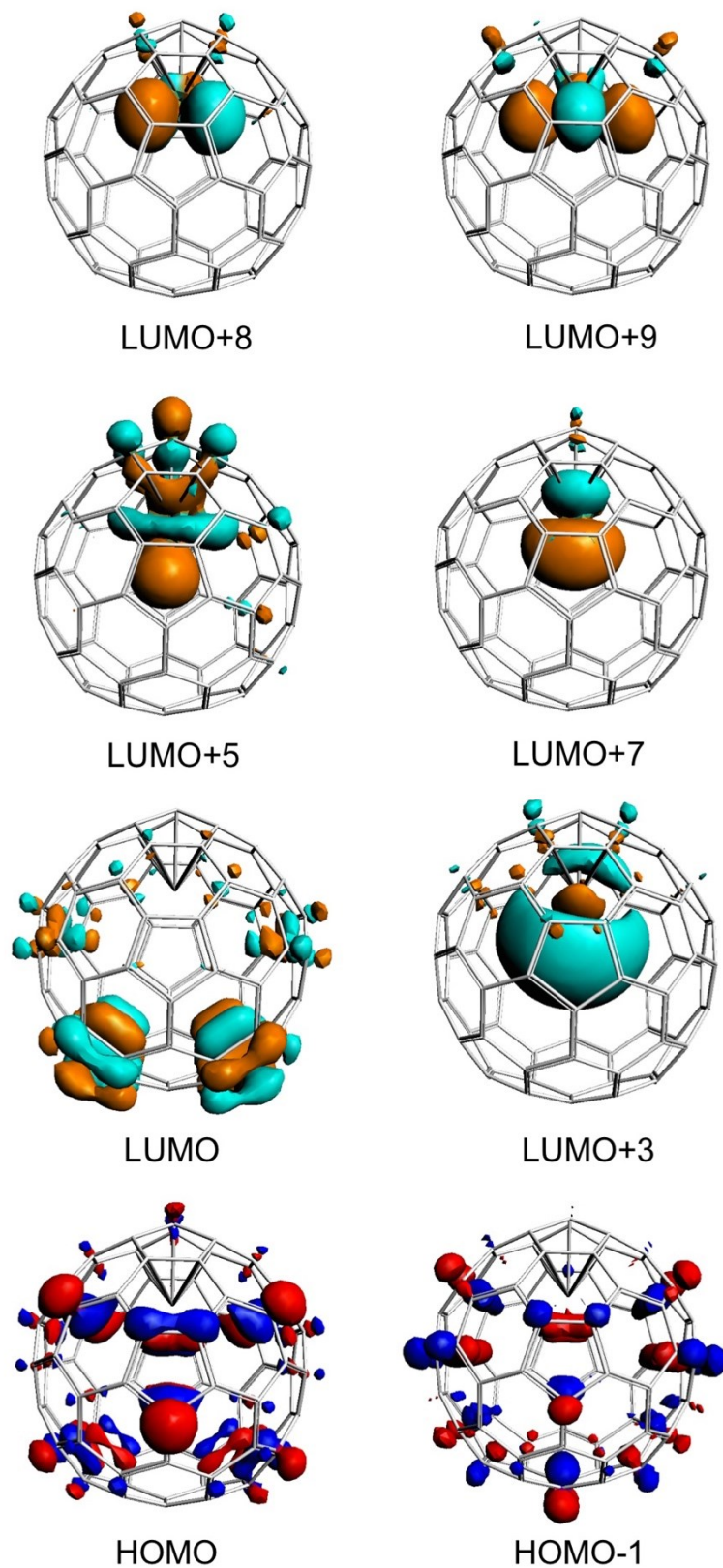
Fig. S4 Frontier molecular orbitals of Th@D_{5h}(6)-C_{80}. Occupied orbitals are localized in the carbon cage; valence Th orbitals (7s, 6d and 5f) are empty.
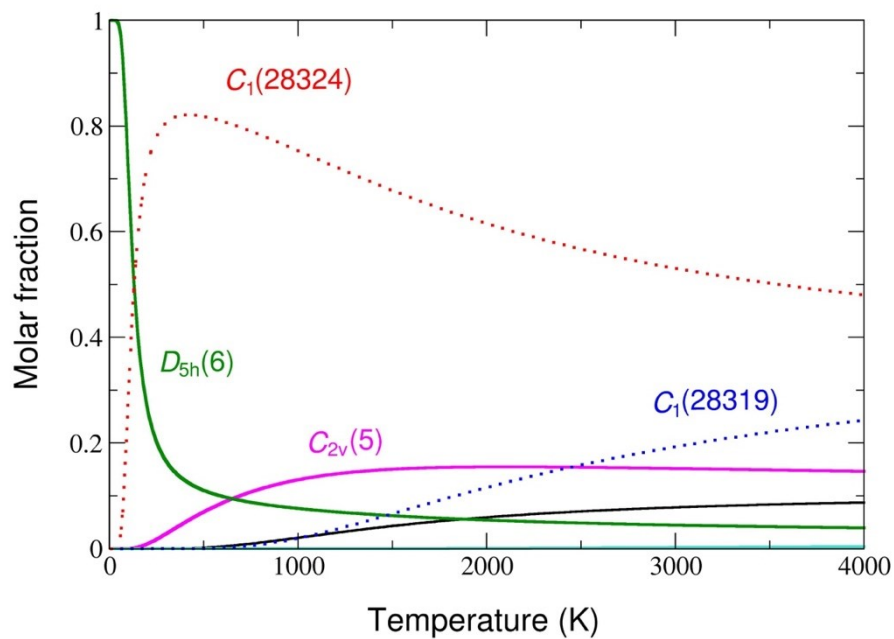
Fig. S5 Molar fractions at different temperatures computed with the FEM approximation for some Th@C_{80} isomers: D_{5h}(6) (green line), C_{2v}(5) (magenta line), C_{2v}(3) (black line), I_h(7) (cyan line), C_1(28324) (red dotted line) and C_1(28319) (blue dotted line).

Metal-to-cage mode

Breathing mode

145 (**150**) cm^{-1}

214 (**219**) cm^{-1}
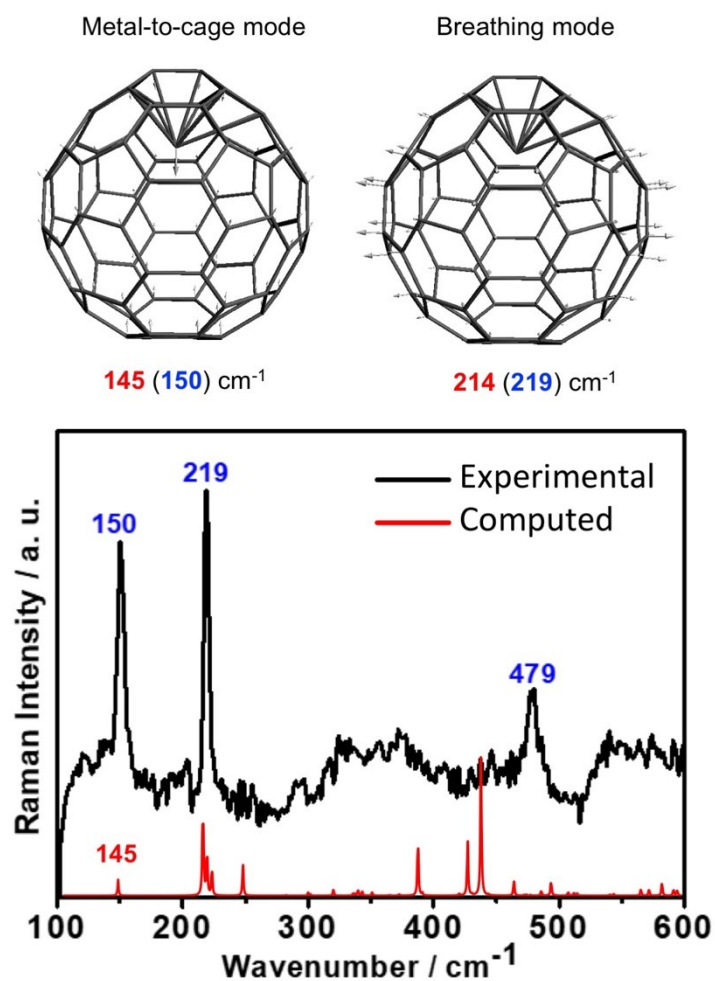
Fig. S6 Computed Raman spectrum for Th@D_{5h}(6)-C$_{80}$ (red line) along with the experimental one (black line). The metal-to-cage normal mode at 150 cm^{-1} (computed at 145 cm^{-1}) and a breathing normal mode at 219 cm^{-1} (computed at 214 cm^{-1}) are represented.

Optimized structure (PBE0/TZP) of Th@D_{5h}(6)-C$_{80}$ (xyz coordinates)

```
    81
Th@D5h(6)-C80
C      2.477152     3.397779     0.727691
C      1.211200     3.650821     1.407706
C      1.162051     2.800209     2.570732
C      2.314871     1.964362     2.571889
C      3.115231     2.277218     1.412139
C      2.477152     3.397779    -0.727691
C      1.211200     3.650821    -1.407706
C     -0.046579     3.968950    -0.730503
C     -0.046579     3.968950     0.730503
C     -1.242914     3.609516     1.409641
C     -1.262912     2.845408     2.643601
C     -0.062870     2.387250     3.217933
C     -0.047894     1.152998     3.918445
C      1.116304     0.306645     3.919000
C      2.295266     0.671570     3.219054
C      3.099597    -0.329714     2.643371
C      3.819446    -0.074223     1.408701
C      3.803276     1.177478     0.731500
C      3.803276     1.177478    -0.731500
C      3.115231     2.277218    -1.412139
C      2.314871     1.964362    -2.571889
C      1.162051     2.800209    -2.570732
C     -0.062870     2.387250    -3.217933
C     -1.262912     2.845408    -2.643601
C     -1.242914     3.609516    -1.409641
C     -2.436811     3.259774    -0.693721
C     -2.436811     3.259774     0.693721
C     -3.153269     2.244615     1.420895
C     -2.432497     2.005828     2.635152
C     -2.396898     0.708809     3.233808
C     -1.204892     0.309923     3.920125
C     -0.761973    -1.051962     3.926221
C      0.669489    -1.054412     3.920407
C      1.415464    -2.066011     3.234175
C      2.660579    -1.700393     2.635045
C      3.109498    -2.312581     1.420855
C      3.853752    -1.318577     0.693671
C      3.853752    -1.318577    -0.693671
C      3.819446    -0.074223    -1.408701
C      3.099597    -0.329714    -2.643371
C      2.295266     0.671570    -3.219054
```

C	1.116304	0.306645	-3.919000
C	-0.047894	1.152998	-3.918445
C	-1.204892	0.309923	-3.920125
C	-2.396898	0.708809	-3.233808
C	-2.432497	2.005828	-2.635152
C	-3.153269	2.244615	-1.420895
C	-3.830226	1.193188	-0.733385
C	-3.830226	1.193188	0.733385
C	-3.899703	-0.056077	1.414543
C	-3.174945	-0.300509	2.618451
C	-2.725738	-1.693659	2.616937
C	-1.495777	-2.060649	3.228153
C	-0.768461	-3.118568	2.617653
C	0.694891	-3.117262	2.619293
C	1.150574	-3.731792	1.414645
C	2.317085	-3.280416	0.733230
C	2.317085	-3.280416	-0.733230
C	3.109498	-2.312581	-1.420855
C	2.660579	-1.700393	-2.635045
C	1.415464	-2.066011	-3.234175
C	0.669489	-1.054412	-3.920407
C	-0.761973	-1.051962	-3.926221
C	-1.495777	-2.060649	-3.228153
C	-2.725738	-1.693659	-2.616937
C	-3.174945	-0.300509	-2.618451
C	-3.899703	-0.056077	-1.414543
C	-3.924926	-1.304041	-0.685693
C	-3.924926	-1.304041	0.685693
C	-3.166803	-2.305019	1.414302
C	-2.383260	-3.280391	0.730555
C	-1.214272	-3.725784	1.414182
C	-0.028766	-4.139666	0.685949
C	-0.028766	-4.139666	-0.685949
C	1.150574	-3.731792	-1.414645
C	0.694891	-3.117262	-2.619293
C	-0.768461	-3.118568	-2.617653
C	-1.214272	-3.725784	-1.414182
C	-2.383260	-3.280391	-0.730555
C	-3.166803	-2.305019	-1.414302
Th	1.142391	1.516106	0.000000

References

1   O. V. Dolomanov, L. J. Bourhis, R. J. Gildea, J. A. K. Howard and H. Puschmann, *J. Appl. Crystallogr.*, 2009, **42**, 339-341.

2   G. Sheldrick, *Acta Crystallographica Section C*, 2015, **71**, 3-8.

3   M. Yamada, N. Mizorogi, T. Tsuchiya, T. Akasaka and S. Nagase, *Chem. Eur. J.*, 2009, **15**, 9486-9493.

4   R. Valencia, A. Rodríguez-Fortea, A. Clotet, C. de Graaf, M. N. Chaur, L. Echegoyen and J. M. Poblet, *Chem. Eur. J.,* 2009, **15**, 10997-11009.

5   Y. Wang, R. Morales-Martinez, X. Zhang, W. Yang, Y. Wang, A. Rodriguez-Fortea, J. M. Poblet, L. Feng, S. Wang and N. Chen, *J. Am. Chem. Soc.*, 2017, **139**, 5110-5116.

6   W. Cai, L. Abella, J. Zhuang, X. Zhang, L. Feng, Y. Wang, R. Morales-Martinez, R. Esper, M. Boero, A. Metta-Magana, A. Rodriguez-Fortea, J. M. Poblet, L. Echegoyen and N. Chen, *J. Am. Chem. Soc.*, 2018, **140**, 18039-18050.

7   Y. Wang, R. Morales-Martinez, W. Cai, J. Zhuang, W. Yang, L. Echegoyen, J. M. Poblet, A. Rodriguez-Fortea and N. Chen, *Chem. Commun.*, 2019, **55**, 9271-9274.

8   M. Jin, J. Zhuang, Y. Wang, W. Yang, X. Liu and N. Chen, *Inorg. Chem.*, 2019, **58**, 16722-16726.

9   W. Q. Shen, L. P. Bao, S. F. Hu, X. J. Gao, Y. P. Xie, X. F. Gao, W. H. Huang and X. Lu, *Chemistry*, 2018, **24**, 16692-16698.

10 G. te Velde, F. M. Bickelhaupt, E. J. Baerends, C. Fonseca Guerra, S. J. A. van Gisbergen, J. G. Snijders and T. Ziegler, *J. Comput. Chem.*, 2001, **22**, 931-967.

11 M. Ernzerhof and G. E. Scuseria, *J. Comput. Chem.,* 1999, **110**, 5029-5036.

12 S. Grimme, *J. Chem. Phys.*, 2006, **124**, 034108.

13 S. Grimme, S. Ehrlich and L. Goerigk, *J. Comput. Chem.*, 2011, **32**, 1456-1465.

14 J. P. Perdew, K. Burke and M. Ernzerhof, *Phys. Rev. Lett.*, 1996, **77**, 3865-3868.